OPEN ACCESS

University of BRISTOL

Yu, K., Bengtsson, B., Ottersten, P., McNamara, DP., Karlsson, P., & Beach, MA. (2004). Modeling of wide-band MIMO radio channels based on NLoS indoor measurements. *IEEE Transactions on Vehicular Technology*, *53*(3), 655 - 665. [No. 3]. https://doi.org/10.1109/TVT.2004.827164

Peer reviewed version

Link to published version (if available):
10.1109/TVT.2004.827164

Link to publication record in Explore Bristol Research
PDF-document

University of Bristol - Explore Bristol Research
General rights

This document is made available in accordance with publisher policies. Please cite only the published version using the reference above. Full terms of use are available:
http://www.bristol.ac.uk/red/research-policy/pure/user-guides/ebr-terms/

Modeling of Wide-Band MIMO Radio Channels Based on NLoS Indoor Measurements

Kai Yu, *Student Member, IEEE*, Mats Bengtsson, *Member, IEEE*, Björn Ottersten, *Fellow, IEEE*, Darren McNamara, Peter Karlsson, and Mark Beach

***Abstract*—In this paper, we first verify a previously proposed Kronecker-structure-based narrow-band model for nonline-of-sight (NLoS) indoor multiple-input–multiple-output (MIMO) radio channels based on 5.2-GHz indoor MIMO channel measurements. It is observed that, for the narrow-band case, the measured channel coefficients are complex Gaussian distributed and, consequently, we focus on a statistical description using the first- and second-order moments of MIMO radio channels. It is shown that the MIMO channel covariance matrix can be well approximated by the Kronecker product of the covariance matrices, seen from the transmitter and receiver, respectively. A narrow-band model for NLoS indoor MIMO channels is thus verified by these results. As for the wide-band case, it is observed that the average power-delay profile of each element of the channel impulse response matrix fits the exponential decay curve and that the Kronecker structure of the second-order moments can be extended to each channel tap. A wide-band MIMO channel model is then proposed, combining a simple COST 259 single-input–single-output channel model and the Kronecker structure. Monte Carlo simulations are used to generate indoor MIMO channel realizations according to the models discussed. The results are compared with the measured data using the channel capacity and good agreement is found.**

***Index Terms*—Antenna arrays, channel capacity, channel modeling, measured channel data, multipath channels, multiple-input–multiple-output (MIMO) channels.**

I. Introduction

IT IS well known that using antenna arrays at both transmitter and receiver over a multiple-input–multiple-output (MIMO) channel can provide a very high channel capacity as long as the environment has sufficiently rich scattering. Under these circumstances, the channel matrix elements have low correlation and the channel realizations are high rank, leading to a substantial increase in channel capacity. In [1]–[3], the channel capacity for MIMO systems has been investigated theoretically. Many MIMO channel-measurement campaigns have been carried out recently, trying to characterize the MIMO channel and/or the corresponding capacity (see [4]–[11]).

Several techniques have been proposed to utilize the spatial and polarization diversity of MIMO communication channels. These techniques can be divided into two main groups [12], [13]: space–time coding and spatial multiplexing. The space–time coding, in general, assumes no knowledge on the propagation channel at the transmitter. At the receiver, the structure of the space–time code is used to correct the errors. Examples of space–time block coding can be found in [14] and [15] and space–time trellis codes have been discussed in [16]. In [17] and [18], space–time block codes are improved by using nonperfect channel information at the transmitter. The spatial multiplexing, on the other hand, attempts to utilize parallel spatial subchannels by exploiting channel information at the receiver. It is well known [1], [19] that when the transmitter has full knowledge about the channel, by using waterfilling [20] to allocate the power for each transmit element, maximum channel capacity can be achieved.

Since the channel capacity is determined by the radio propagation conditions of MIMO channel, there is, of course, great interest in characterizing and modeling MIMO radio channels for different environments. With the help of accurate MIMO radio channel models, high-performance MIMO communication systems can be designed and system performance can be accurately predicted. Furthermore, accurate MIMO radio channel models can assist in the design of space–time codes or spatial multiplexing techniques under different scenarios. Several channel models have been reported for single-input–single-output (SISO) channels, e.g., [21]–[26]. The single-input–multiple-output (SIMO) and multiple-input–single-output (MISO) channels have also been studied and different models have been proposed (see [27] and the references therein). Extending these models to the MIMO case, however, is not straightforward, since the spatial characteristics now have to be considered at both ends, either directly or indirectly.

In the field of MIMO channel modeling, a so-called one-ring model has been proposed and investigated in [28]. In [29], a distributed scattering model has been reported in order to explain the pinhole phenomenon [30] that may appear in outdoor scenarios. A model based on channel power correlation coefficients has been presented in [31] and is extended to include the complex valued correlation matrix in [32]. For a detailed review on MIMO wireless channel models, see [33]. However, models based on experimental data are still rare. To the authors' knowledge, no wide-band MIMO channel model based on measured MIMO data has been published until now.

Manuscript received November 1, 2002; revised March 19, 2003 and December 12, 2003. This work was conducted in part within the Smart Antenna Technology in Universal Broadband Wireless Networks (SATURN) Project funded by the European Union Information Society Technology Program. This paper was presented in part at the IEEE Global Telecommunications Conference, November 2001, and at the IEEE Vehicular Technology Conference, May 2002.

K. Yu, M. Bengtsson, and B. Ottersten are with the Department of Signals, Sensors, and Systems, Royal Institute of Technology, Stockholm SE-100 44, Sweden (e-mail: kaiyu@s3.kth.se).

D. McNamara and M. Beach are with Centre for Communication Research, University of Bristol, Bristol BS8 1UB, U.K.

P. Karlsson is with TeliaSonera Sweden, Mobile Network R&D, Malmö SE-20120, Sweden.

Digital Object Identifier 10.1109/TVT.2004.827164

0018-9545/04$20.00 © 2004 IEEE

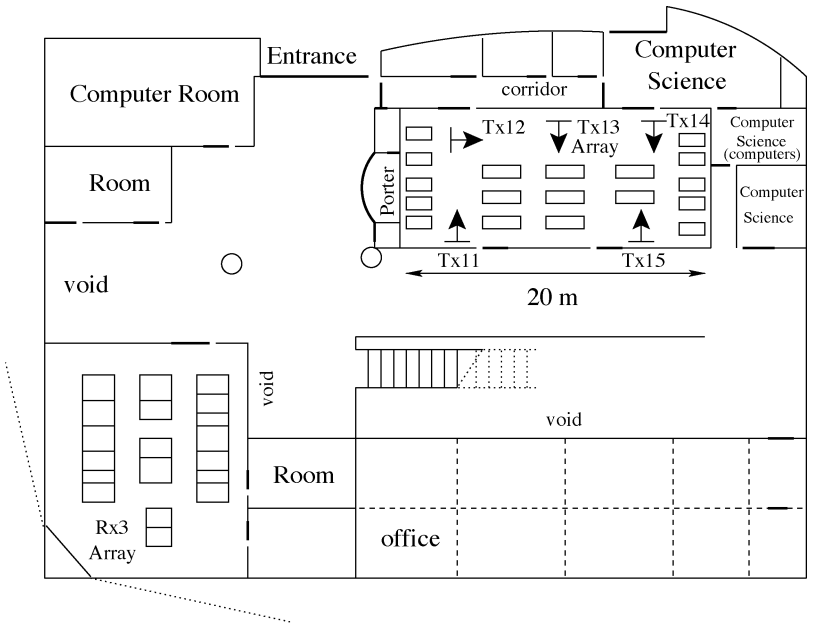

Fig. 1. Measurement scenario for the NLoS indoor MIMO channels.

This paper reports results based on data measured by the University of Bristol, Bristol, U.K., as part of the European Union IST Smart Antenna Technology in Universal Broadband Wireless Networks (SATURN) project. First, a Kronecker-structure-based narrow-band MIMO channel model is verified. We then further extend this model to the wide-band case based on the same sets of data. These two models have been assumed in several papers [34]–[36] in order to analyze channel capacity, simulate MIMO system, and predict its performance. This paper is organized as follows. Section II gives a brief description of the whole measurement including the measurement scenario, the measurement equipments, and the corresponding parameter settings. A least-squares Kronecker factorization method is described in Section III and will be used in the following sections. Section IV analyzes the measured data and verifies a statistical narrow-band channel model for the nonline-of-sight (NLoS) indoor MIMO radio channels. In Section V, the measured wide-band NLoS indoor MIMO channel realizations are studied and a wide-band MIMO channel model is proposed. Finally, the conclusions and discussion are given in Section VI.

II. Measurement Description

The measurement site was the Merchant Venturers Building, University of Bristol. The general layout of the test site includes office rooms, computer labs, corridors, and open spaces. The entire set of measurements includes 15 transmitter locations and three receiver locations. Both line-of-sight (LoS) and NLoS scenarios were measured [37]. In this paper, we focus on modeling an NLoS scenario as shown in Fig. 1, which includes five transmit positions and one receive position. In this figure, the arrow at each transmitter location indicates the orientation of the transmit array. The transmitter was located in a computer laboratory and the receiver was located in a large modern office with cubicles.

The Medav RUSK BRI vector sounder was used during the measurements, with eight-element uniform linear arrays at both the transmit and receive sides. The transmit elements were omnidirectional and can transmit up to 27 dBm to the receiver. The receive elements had a beamwidth of 120° (for pictures, see [4]). The distance between two neighboring antenna elements was 0.5λ for both arrays. There was feedback from the receiver to the transmitter by a cable in order to synchronize the transmitter and receiver.

The measurements were centered at 5.2 GHz. To measure the channel realizations, a periodic multifrequency signal with 120-MHz bandwidth was sent out by the transmit elements and was captured by the receive elements. For each transmitter and receiver pair, the signal-to-noise ratio (SNR) was above 20 dB. The receiver downconverted the received signal to 80 MHz, which was sampled at 320 MHz. The wide-band channel response was then estimated and saved in the frequency domain. During the measurements, the maximum expected channel excess delay was set as 800 ns, corresponding to 97 frequency subchannels.

For each transmit element, one "vector snapshot" (i.e., one measurement from each receive element) was taken by the receiver through switching control circuitry. One MIMO snapshot included eight vector snapshots since there were eight transmit elements. The overall sampling time for one MIMO snapshot was 102.4 μs, which is well within the coherence time of this indoor scenario.

For each transmitter and receiver pair, one complete measurement includes 199 time blocks with 16 MIMO snapshots within each block; hence, there were, overall 3184, complete MIMO snapshots for each frequency subchannel. Since the time delay between two neighboring blocks was 26.624 ms, this means that the total time for one complete measurement was 5.3 s. In total, five complete measurements were conducted for the measured NLoS scenarios. During the measurements, people were moving around both at the transmitter and receiver as normal.

It is observed that even though people were moving around during the measurements, the time variations on a single link of

each narrow-band subchannel are still very small, leading to a low mobility scenario. Therefore, in this paper, pairs of two and three neighboring elements have been used as examples, with different subsets of elements being selected in order to get sufficiently many MIMO channel realizations to analyze the statistics of the measured channel. The idea is that small dislocations of the antenna arrays (corresponding to selecting different subsets of the eight element array) give different MIMO channel realizations with the same statistics. Furthermore, in the narrow-band case, the snapshots from different frequency subchannels are also treated as different channel realizations. Note that we only focus on modeling the channel with moderate array sizes. For large array sizes, a physical model appears to be a good candidate, since the physical parameters are easier to identify using antenna arrays with large aperture. In the following sections, unless otherwise stated, the data measured at Tx13-Rx3 are used as an example. Similar results are found for the other four transmitter locations (see Fig. 1).

III. Least-Squares Kronecker Factorization

In [38] and [39], a least-squares Kronecker factorization method has been introduced to approximate a complex valued matrix $\mathbf{R}$ with the Kronecker product of two complex valued matrices $\mathbf{X}$ and $\mathbf{Y}$ optimally (with suitable dimensions). This method will be used in the following two sections to factorize the measured MIMO channel covariance matrices. A brief description of the least-squares Kronecker factorization method is given as follows.

The original problem boils down to solving the minimization problem

$$\arg\min_{\mathbf{X},\mathbf{Y}} \|\mathbf{R}-\mathbf{X}\otimes\mathbf{Y}\|_F \tag{1}$$

where $\|\cdot\|_F$ denotes the Frobenius norm and $\otimes$ is the Kronecker product.

This can be solved by rearranging the positions of the matrix elements, which leads to a permuted version of the original problem [38], i.e.,

$$\arg\min_{\mathbf{X},\mathbf{Y}} \left\|\mathbf{R}_{\text{perm}}-\text{vec}(\mathbf{X})\,(\text{vec}(\mathbf{Y}))^T\right\|_F \tag{2}$$

where $(\cdot)^T$ denotes transpose, $\text{vec}(\cdot)$ is the vec-operator and $\mathbf{R}_{\text{perm}}$ is the permuted matrix. Note that the original problem (1) and its permuted version (2) are equivalent since the Frobenius norm is not affected by permutation. More details on how to find the permuted version of the original problem can be found in the Appendix.

The well-known solution to this least-squares rank-one approximation of $\mathbf{R}_{\text{perm}}$ in (2) can easily be obtained using the singular value decomposition (SVD) [40], i.e.,

$$\text{vec}(\mathbf{X}) = \gamma\mathbf{u}_{\max} \tag{3}$$

$$(\text{vec}(\mathbf{Y}))^c = \gamma^{-1}\sigma_{\max}\mathbf{v}_{\max} \tag{4}$$

where $(\cdot)^c$ denotes the complex conjugate, $\sigma_{\max}$ is the largest singular value of $\mathbf{R}_{\text{perm}}$, $\mathbf{u}_{\max}$ and $\mathbf{v}_{\max}$ are the left and right singular vector associated with $\sigma_{\max}$, and γ is an arbitrary scalar. Although, in general, $\mathbf{u}_{\max}$ and $\mathbf{v}_{\max}$ are not unique [41], it can be shown [39] that the solution $\mathbf{X}$ and $\mathbf{Y}$ can always be chosen to be Hermitian positive definite if $\mathbf{R}$ is Hermitian positive definite.

IV. Narrow-Band MIMO Channel Model

In this section, we focus on modeling MIMO radio channels from a narrow-band system perspective, i.e., we assume that the channel has a constant response over the entire system bandwidth. Note that the narrow-band MIMO channel model verified in this section can also be seen as a special case of the wide-band MIMO channel model, which will be presented in the next section, with only a single tap.

A. Capacity and Second-Order Moments

Assume there are M transmit elements and N receive elements. For a narrow-band MIMO channel, the input–output relationship can be expressed in the baseband as

$$\mathbf{y} = \mathbf{H}\mathbf{s} + \mathbf{n} \tag{5}$$

where $\mathbf{s}$ is the transmitted signal, $\mathbf{y}$ is the received signal, and $\mathbf{n}$ is additive white Gaussian noise (AWGN). The channel matrix $\mathbf{H}$ here is an $N \times M$ matrix.

For a fixed channel realization, the channel capacity, under the constraint that the transmitter has no channel state information and the transmitted power is equally allocated to each transmit element, can be expressed as [2]

$$C = \log_2 \det\left(\mathbf{I}_N + \frac{\rho}{M}\mathbf{H}\mathbf{H}^H\right) \text{ bits/s/Hz} \tag{6}$$

where $(\cdot)^H$ denotes Hermitian transpose, $\mathbf{H}$ is the $N \times M$ normalized channel matrix, and ρ is the average SNR at each receiver branch. To calculate the channel capacity and statistics, the measured channel matrices $\mathbf{H}$ should be correctly normalized. We use the same normalization factor for all the measured channel realizations such that

$$\text{E}\left(\|\mathbf{H}\|_F^2\right) = NM \tag{7}$$

where $\text{E}(\cdot)$ denotes the expected value, which averages over all measured MIMO channel realizations for a specific transmitter and receiver pair.

Define the normalized transmitter, receiver, and channel covariance matrices as

$$\mathbf{R}_H^{Tx} = \text{E}\left[\left(\mathbf{h}_i^H\mathbf{h}_i\right)^T\right], \quad \text{for } i = 1,\ldots,N \tag{8}$$

$$\mathbf{R}_H^{\text{Rx}} = \text{E}\left[\mathbf{h}^j\mathbf{h}^{jH}\right], \quad \text{for } j = 1,\ldots,M \tag{9}$$

$$\mathbf{R}_H = \text{E}\left[\text{vec}(\mathbf{H})\text{vec}^H(\mathbf{H})\right] \tag{10}$$

where $\mathbf{h}_i$ is the ith row of $\mathbf{H}$, $\mathbf{h}^j$ is the jth column of $\mathbf{H}$, and $\mathbf{H}$ is the channel matrix normalized according to (7). It was conjectured in [28] and [42] that the normalized MIMO channel covariance matrix can be well approximated by the Kronecker product of the covariance matrices at the transmitter and receiver, i.e.,

$$\mathbf{R}_H = \mathbf{R}_H^{\text{Tx}} \otimes \mathbf{R}_H^{\text{Rx}}. \tag{11}$$

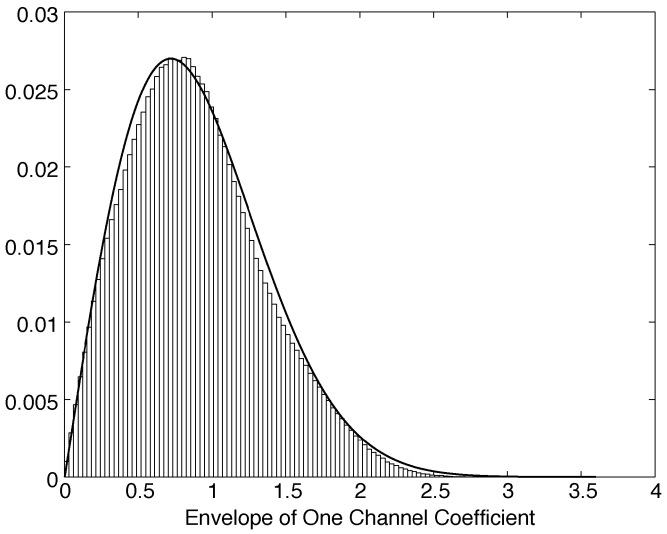

Fig. 2. Histogram of the envelope of one channel coefficient for an NLoS indoor MIMO scenario and a Rayleigh pdf (normalized).

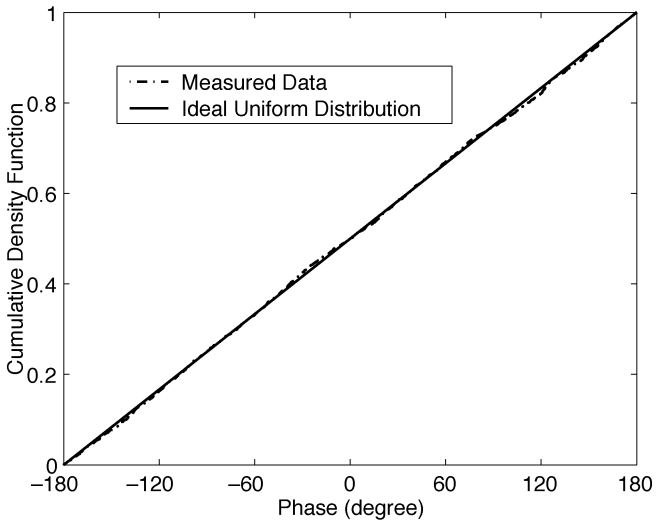

Fig. 3. The cdf of the phase of one channel coefficient for an NLoS indoor MIMO scenario and the uniform distribution curve over $[-\pi, \pi]$.

Below, this Kronecker structure will be verified from the measured data. Note that in [43], the same structure was proposed where the amplitude correlation was verified using the wireless system engineering (WiSE) ray-tracing simulator.

B. Measurement Results

1) Distribution of the Channel Coefficients: First, we investigate the distribution of the channel coefficients. Fig. 2 shows the normalized histogram of the envelope of one channel coefficient along with a Rayleigh probability density function (pdf). It is clearly observed that the envelope of the channel coefficient has a good fit with a Rayleigh distribution. By plotting the cumulative density function (cdf) in Fig. 3, the phase of the channel coefficient appears to be uniformly distributed over $[-\pi, \pi]$. Furthermore, the K factor is estimated as the ratio of the specular power and the power of multipath components [44], [45]. The corresponding results are smaller than -30 dB for all five data sets, which proves that no dominant components exist for these measured scenarios. We conclude that the channel coefficients for these measured NLoS indoor MIMO scenarios appear to be zero-mean complex Gaussian.

2) Second-Order Moments: It is well known that a complex Gaussian random process is completely characterized by its first- and second-order moments [46]. To investigate the second-order statistics for these NLoS indoor scenarios, we define the following narrow-band model error Ψ to evaluate the difference between two matrices $\mathbf{A}_1$ and $\mathbf{A}_2$:

$$\Psi(\mathbf{A}_1, \mathbf{A}_2) = \frac{\|\mathbf{A}_1 - \mathbf{A}_2\|_F}{\|\mathbf{A}_1\|_F}. \tag{12}$$

For a 2×2 setup, the estimated transmit, receive, and channel covariance matrices for Tx13-Rx3 are shown at the bottom of the page and as follows:

$$\hat{\mathbf{R}}_H^{\mathrm{Tx}} = \begin{bmatrix} 0.995 & 0.010 - j0.037 \\ 0.010 + j0.037 & 1.005 \end{bmatrix}$$
$$\hat{\mathbf{R}}_H^{\mathrm{Rx}} = \begin{bmatrix} 0.985 & 0.694 + j0.195 \\ 0.694 - j0.195 & 1.015 \end{bmatrix}$$

where the $\hat{(\cdot)}$ indicates a sample estimate of the corresponding quantities in (8)–(10). Clearly, the correlation at the receive side is much higher than the correlation at the transmit side. This could be due to the fact that the transmit elements were omnidirectional while the receive elements could only receive the signal within 120° range and, therefore, more scatterers can be "seen" at the transmitter than at the receiver. We also note that, for different transmit locations, the corresponding covariance matrices have small differences.

In order to see how well the estimated MIMO channel covariance matrix $\hat{\mathbf{R}}_H$ can be approximated by a Kronecker product of $\hat{\mathbf{R}}_H^{\mathrm{Tx}}$, $\hat{\mathbf{R}}_H^{\mathrm{Rx}}$, we use the least-squares Kronecker factorization method to factorize $\hat{\mathbf{R}}_H$ optimally into two Hermitian positive definite submatrices $\mathbf{X}$ and $\mathbf{Y}$ and compare the results with the sample covariance estimates. Here, since γ in (3) and (4) is an arbitrary scalar, the least-squares method has been used to find γ, which minimizes the differences between $\mathbf{X}$, $\mathbf{Y}$ and $\hat{\mathbf{R}}_H^{\mathrm{Tx}}$, $\hat{\mathbf{R}}_H^{\mathrm{Rx}}$, respectively. From the measured data, we investigate two narrow-band model errors, i.e., the error from the least-squares Kronecker factorization and the error from the sample covariance estimates. The results from the data measured between Tx13-Rx3 are listed in the first two rows of Table I. We also

$$\hat{\mathbf{R}}_H = \begin{bmatrix} 0.991 & 0.683 + j0.205 & 0.018 - j0.005 & 0.033 - j0.079 \\ 0.683 - j0.205 & 1.000 & 0.009 + j0.018 & 0.002 - j0.069 \\ 0.018 + j0.005 & 0.009 - j0.018 & 0.979 & 0.706 + j0.186 \\ 0.033 + j0.079 & 0.002 + j0.069 & 0.706 - j0.186 & 1.030 \end{bmatrix}$$

TABLE I
NARROW-BAND MODEL ERRORS (Tx13–Rx3)

	2×2	3×3
$\Psi(\hat{\mathbf{R}}_H, \mathbf{X}\otimes\mathbf{Y})$	0.76 %	4.52 %
$\Psi(\hat{\mathbf{R}}_H, \hat{\mathbf{R}}_H^{Tx}\otimes\hat{\mathbf{R}}_H^{Rx})$	0.86 %	4.79 %
$\Psi(\hat{\mathbf{R}}_H^{Tx}, \mathbf{X})$	0.40 %	1.74 %
$\Psi(\hat{\mathbf{R}}_H^{Rx}, \mathbf{Y})$	0.03 %	1.60 %

TABLE II
NARROW-BAND MODEL ERRORS (3 × 3 SETUP)

	$\Psi(\hat{\mathbf{R}}_H, \mathbf{X}\otimes\mathbf{Y})$	$\Psi(\hat{\mathbf{R}}_H, \hat{\mathbf{R}}_H^{Tx}\otimes\hat{\mathbf{R}}_H^{Rx})$
Tx11	7.26 %	7.57 %
Tx12	6.64 %	7.33 %
Tx13	4.52 %	4.79 %
Tx14	7.00 %	7.68 %
Tx15	4.65 %	4.94 %

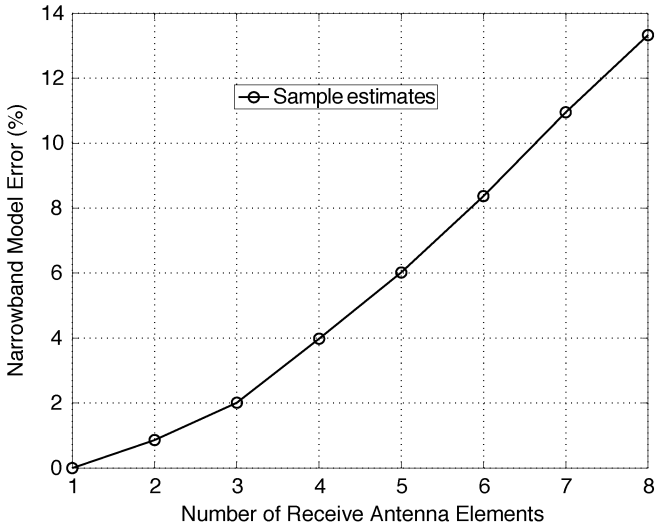

Fig. 4. Narrow-band model errors with two transmit antenna elements and 1–8 receive antenna elements.

note that the differences between the matrices $\mathbf{X}$, $\mathbf{Y}$ and the covariance matrices $\hat{\mathbf{R}}_H^{\mathrm{Tx}}$, $\hat{\mathbf{R}}_H^{\mathrm{Rx}}$ are small, as shown in the last two rows of Table I.

For the other transmitter locations, similar narrow-band model errors have been found. Table II lists the narrow-band model errors for all five transmitter locations with a 3 × 3 setup.

From Tables I and II, it is clearly shown that the MIMO channel covariance matrix can be well modeled as shown in (11). The narrow-band model errors are well below 10% and the model errors from the sample estimates are close to those from the optimal Kronecker factorization. Reasonably small narrow-band model errors are found with the number of antenna elements up to five at both ends. However, the narrow-band model error increases when the number of antenna elements increases. Fig. 4 shows that with two transmit antenna elements, increasing the number of receive antenna elements will also increase the narrow-band model errors. Similar observations are found when the number of transmit antenna elements increases. One possible explanation is that fewer channel realizations are obtained from the spatial averaging when the number of antenna elements increases. Nevertheless, it is fair to conclude

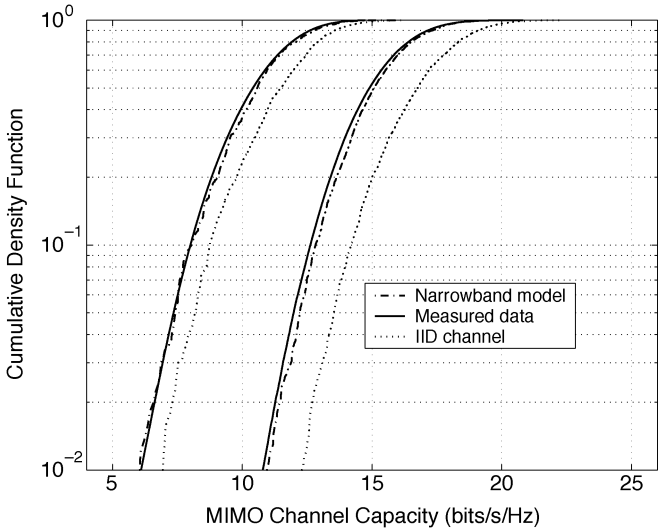

Fig. 5. The cdf of the narrow-band channel capacity from the measured data, narrow-band channel model, and i.i.d. MIMO channel. Power is equally allocated to the transmit elements and the SNR at the receive side is 20 dB.

that this Kronecker structure of the channel covariance matrix (11) is suitable for arrays with a moderate number of elements under these conditions.

C. Narrow-Band MIMO Channel Model

Given a complex Gaussian channel and the Kronecker structure of MIMO channel covariance matrix (11), the MIMO channel matrix can be modeled as [28], [34]

$$\mathbf{H} = \left(\mathbf{R}_H^{\mathrm{Rx}}\right)^{\frac{1}{2}} \mathbf{G} \left[\left(\mathbf{R}_H^{\mathrm{Tx}}\right)^{\frac{1}{2}}\right]^T \tag{13}$$

where the stochastic $N \times M$ matrix $\mathbf{G}$ contains independent and identically distributed (i.i.d.) $\mathcal{CN}(0,1)$ elements and $(\cdot)^{1/2}$ is defined such that $\mathbf{R}^{1/2}(\mathbf{R}^{1/2})^H = \mathbf{R}$.

Using the well-known properties of the Kronecker product [47], it is easy to show that the MIMO channel covariance matrix of (13) can be decoupled as in (11). This means that given a zero-mean complex Gaussian process and its second-order moments (11), the MIMO channel model (13) is uniquely determined since a complex Gaussian process is completely specified by its first- and second-order moments. However, if the channel is not Gaussian, then the channel model is not unique. A simple example can be found in [48], which shows that a low-rank channel model can generate exactly the same second-order moments (11).

Using Monte Carlo computer simulations, 1000 channel realizations are generated and the cdf of the simulated channel capacity is compared with that from the measured data. The results for the 2 × 2 and 3 × 3 cases are given in Fig. 5. As a reference, the capacity for the i.i.d. channel is also included. From this figure, it is shown that the channel capacity obtained from the measured channel can be well simulated by the model.

V. WIDE-BAND MIMO CHANNEL MODEL

The narrow-band channel model described in the previous section assumes that the system bandwidth is narrow enough so that the frequency response can be treated as a complex valued

scalar over the whole bandwidth, the so-called frequency-flat channel. In many communication systems, however, the bandwidth is significant and the channel is frequency dependent due to the multipath characteristics of the propagation channels. Such frequency-selective channels may cause intersymbol interference (ISI). Therefore, it is of great importance to have accurate wide-band MIMO channel models in order to predict wide-band MIMO channel capacity and to evaluate different methods proposed to solve the ISI problem. In this section, we present a wide-band MIMO channel model that combines a simple COST 259 SISO channel model with the Kronecker structure of the second-order moments. The wide-band channel model will be used to simulate a MIMO channel with 120-MHz bandwidth and the channel capacity will be compared with that from the measured data.

A. Wide-Band Channel Capacity

Consider a wide-band MIMO system with M transmit elements and N receive elements. The baseband input–output relationship is given by

$$\mathbf{y}(\tau) = \mathbf{H}(\tau) * \mathbf{s}(\tau) + \mathbf{n}(\tau) \tag{14}$$

where $\mathbf{s}(\tau)$ is the transmitted signal, $\mathbf{y}(\tau)$ is the received signal, $\mathbf{n}(\tau)$ is AWGN, and * denotes convolution. Each element of the channel impulse response matrix $\mathbf{H}(\tau)$ is the impulse response from a transmit antenna to a receive antenna.

When the transmitted power is equally allocated to each transmit element and frequency subchannel, the wide-band channel capacity can be expressed as [3], [49]

$$C = \int_W \log_2 \det\left(\mathbf{I}_N + \frac{\rho}{M}\mathbf{H}(f)\mathbf{H}^H(f)\right) df \text{ bits/s} \tag{15}$$

where W is the overall bandwidth of the MIMO channel, $\mathbf{H}(f)$ is the normalized frequency response matrix of each narrow-band subchannel, and ρ is the average SNR at each receiver branch over the entire bandwidth. Here, we normalize the frequency response of every narrow-band subchannel using a common factor such that

$$\int_W \mathrm{E}\left(||\mathbf{H}(f)||_F^2\right) df = \mathrm{WNM}. \tag{16}$$

B. Average Power-Delay Profile and Root-Mean-Square (rms) Delay Spread

As stated in Section II, the measured data were stored in the frequency domain and, therefore, we use the inverse Fourier transform to regenerate the MIMO channel impulse response matrix. Hanning windowing is used to lower the sidelobe effects.

To show how the received power changes according to a fixed time delay reference, the average power-delay profile is found by averaging the instantaneous power-delay profiles over the whole measurement time.

The rms delay spread is a measure of how dispersive the channel is. It is defined as the square root of the second central moment and can be calculated as [45]

$$\overline{\sigma}_\tau = \sqrt{\bar{\tau^2} - (\bar{\tau})^2} \tag{17}$$

where

$$\bar{\tau} = \frac{\sum_l |a_l|^2 \tau_l}{\sum_l |a_l|^2} \tag{18}$$

and

$$\bar{\tau^2} = \frac{\sum_l |a_l|^2 \tau_l^2}{\sum_l |a_l|^2} \tag{19}$$

are the first (also called "mean excess delay") and second moments of the instantaneous power-delay profile, respectively. Here, l is the tap index, a_l is the complex tap amplitude, and τ_l is the time delay relative to the first detected signal.

C. Second-Order Moments

For a wide-band MIMO channel, the normalized transmit, receive, and channel covariance matrices associated with the lth tap are defined as

$$\mathbf{R}_{\mathrm{Tx}}^l = \mathrm{E}\left[\left(\left(\mathbf{h}_i^l\right)^H \mathbf{h}_i^l\right)^T\right], \quad \text{for } i = 1, \ldots, N \tag{20}$$

$$\mathbf{R}_{\mathrm{Rx}}^l = \mathrm{E}\left[\mathbf{h}_l^j \left(\mathbf{h}_l^j\right)^H\right], \quad \text{for } j = 1, \ldots, M \tag{21}$$

$$\mathbf{R}_H^l = \mathrm{E}\left[\mathrm{vec}(\mathbf{H}_l)\mathrm{vec}(\mathbf{H}_l)^H\right] \tag{22}$$

where $\mathbf{h}_i^l$ is the ith row of $\mathbf{H}_l$, $\mathbf{h}_l^j$ is the jth column of $\mathbf{H}_l$, and $\mathbf{H}_l$ is the lth tap of the channel impulse response matrix and is normalized according to (7). It is of great interest to see whether the Kronecker structure (11) can be extended to each channel tap, i.e., if

$$\mathbf{R}_H^l = \mathbf{R}_{\mathrm{Tx}}^l \otimes \mathbf{R}_{\mathrm{Rx}}^l. \tag{23}$$

Note that this extension of the Kronecker structure has also been discussed and filed in the Third Generation Partnership Project (3GPP) meetings [50].

D. Measurement Results

1) Average Power-Delay Profile and rms Delay Spread: The average power-delay profile of one element of the channel impulse response matrix is shown in Fig. 6. It is observed that the curve fits the exponential decay curve quite well. Similar observations were reported in [26] and [51]–[53]. It is further observed that the power-delay profile varies from one transmit location to another and, therefore, is location dependent. The rms delay spread is calculated for each instantaneous power-delay profile by setting the threshold to be 20 dB below the peak power [45]. Fig. 7 shows the cdf of the measured rms delay spread. The mean rms delay spread is 36.7 ns in this case. For the other transmitter locations, the mean rms delay spread varies between 30 to 40 ns. These numbers are consistent with the rms values reported in [45], [54], and [55].

Based on the channel variations shown above, assume that each channel tap is independent zero-mean complex Gaussian.

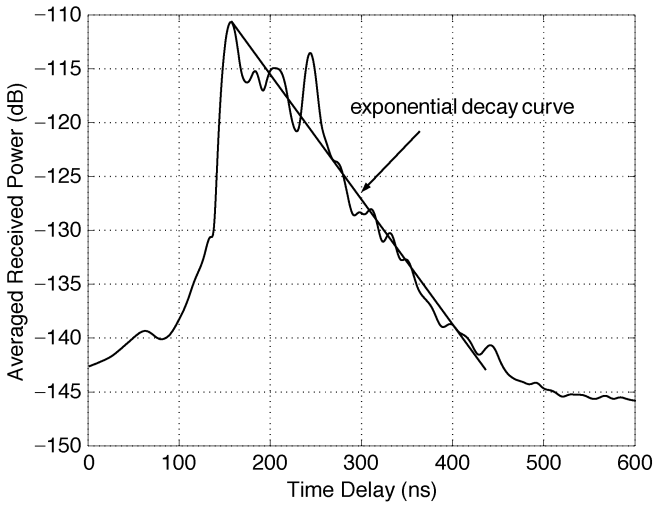

Fig. 6. Average power-delay profile of one element of the channel impulse response matrix.

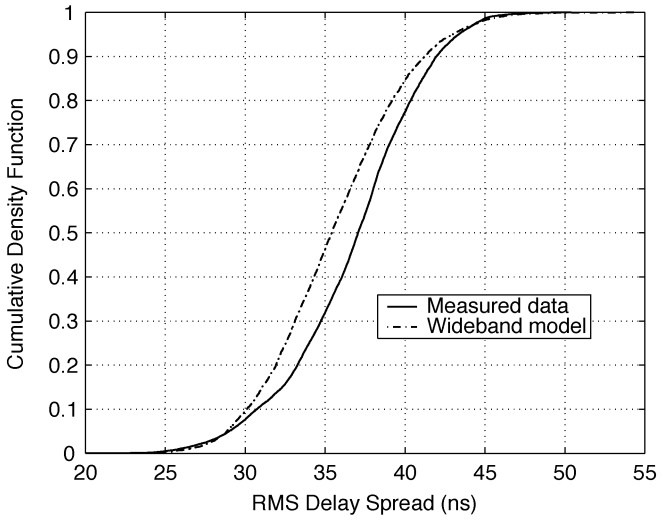

Fig. 7. The cdf of rms delay spread for one element of the channel impulse response matrix from the measured data and wide-band channel model.

The following simple tapped delay line SISO channel model proposed in the European research initiative COST 259 [51] is used to model each elemently of the channel impulse response matrix, i.e.,

$$h(\tau) = \sum_{l=1}^{L} \sqrt{\bar{p}_l} g_l \delta\left[\tau - (l-1)\Delta\tau\right] \tag{24}$$

where $\delta(\cdot)$ is the Dirac delta function, $\Delta\tau$ is the time spacing between neighboring taps, τ is the time delay, and $g_l \in \mathcal{CN}(0,1)$. The average power of the lth tap $\bar{p}_l$ is modeled as

$$\bar{p}_l = Ae^{-\frac{(l-1)\Delta\tau}{2\Gamma}} \tag{25}$$

where Γ is the mean rms delay spread and A is a normalization factor. No Doppler frequency shift is considered here due to the low mobility of the measured scenario. Other SISO channel models, e.g., [24], can also be used as long as they assume that each channel tap is independent zero-mean complex Gaussian. This makes the wide-band MIMO channel model more flexible to have a tradeoff between complexity and accuracy. It is important to note that such a tradeoff always exists when modeling the channel. We will see later that the statistical behavior of each element of the channel impulse response matrix can be well regenerated by this simple channel model.

2) Second-Order Moments: To measure the difference between the normalized MIMO channel covariance matrix $\mathbf{R}_H^l$ and the Kronecker product of two covariance matrices $\mathbf{R}_{\mathrm{Tx}}^l$ and $\mathbf{R}_{\mathrm{Rx}}^l$, the residual $\Psi(\mathbf{R}_H^l, \mathbf{R}_{\mathrm{Tx}}^l \otimes \mathbf{R}_{\mathrm{Rx}}^l)$ defined in (12) is used for each tap. Furthermore, since each tap has a different power, a wide-band model error, Υ is defined to give different weights to each tap according to the average power-delay profile, i.e.,

$$\Upsilon = \sqrt{\frac{\sum_l \bar{p}_l^2 \left\|\mathbf{R}_H^l - \mathbf{R}_{\mathrm{Tx}}^l \otimes \mathbf{R}_{\mathrm{Rx}}^l\right\|_F^2}{\sum_l \bar{p}_l^2 \left\|\mathbf{R}_H^l\right\|_F^2}} \tag{26}$$

where $\bar{p}_l$ is the average power for the lth tap.

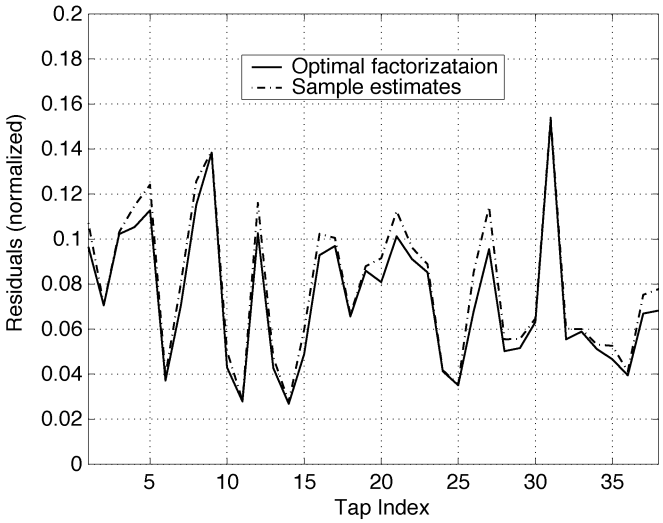

Fig. 8. Residuals of the Kronecker structure (2×2 case).

TABLE III
WIDE-BAND MODEL ERRORS (Υ)

	2×2 setup	3×3 setup
Tx11	4 %	8 %
Tx12	7 %	14 %
Tx13	8 %	19 %
Tx14	8 %	13 %
Tx15	6 %	16 %

Calculating the measured MIMO channel covariance matrix $\hat{\mathbf{R}}_H^l$ and comparing with the Kronecker product of the covariance matrices $\hat{\mathbf{R}}_{\mathrm{Tx}}^l$ and $\hat{\mathbf{R}}_{\mathrm{Rx}}^l$, the results are given in Fig. 8 and Table III. For a 2×2 case, the residuals for each tap are plotted in Fig. 8 along with those from the optimal least-squares Kronecker factorization. Only 38 of 97 successive taps have been plotted, i.e., from approximately 135 ns (the first arrived peak) to 450 ns (the noise floor) in Fig. 6. We note that the residuals from the sample estimates are only slightly larger than the residuals from the least-squares Kronecker factorization. Table III lists the wide-band model errors for different transmit locations

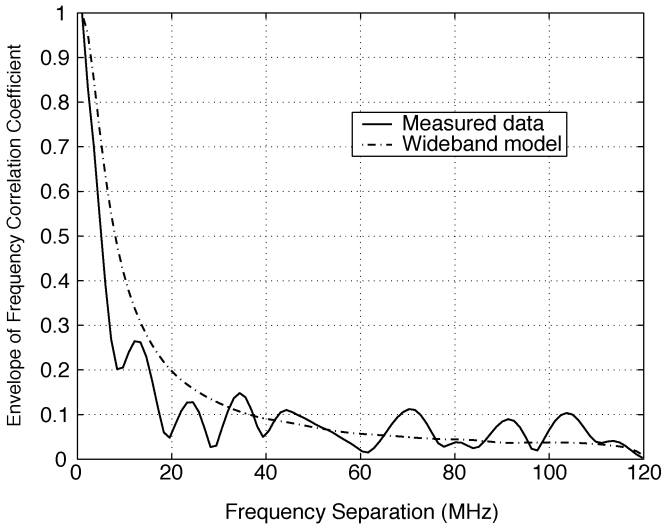

Fig. 9. Averaged frequency correlation function.

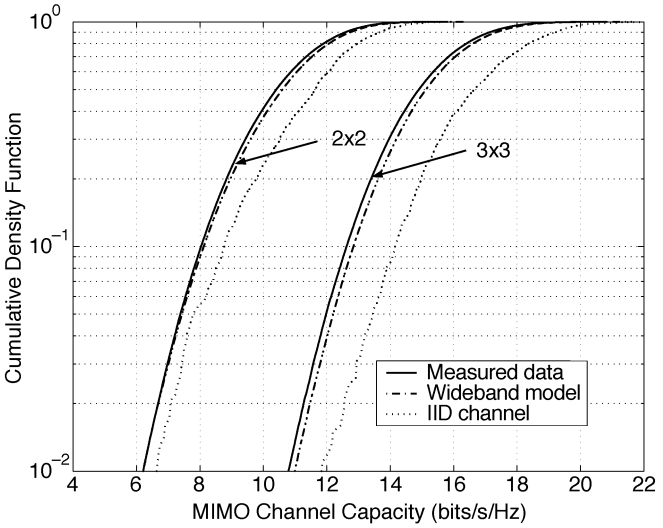

Fig. 10. The cdf of the narrow-band channel capacity. Power is equally allocated and the SNR at the receive side is 20 dB.

and setups. It is shown that the wide-band model errors are below 20% for the worst case. Therefore, we conclude that, for each tap, the normalized MIMO channel covariance matrix can be approximated quite well by the Kronecker structure (23). We will see shortly that both the narrow- and wide-band MIMO channel capacities (simulated based on the above Kronecker structure) agree well with the measured data.

E. Wide-Band MIMO Channel Model

Combining the SISO channel model described before and the Kronecker structure for each tap, the wide-band MIMO channel impulse response matrix $\mathbf{H}(\tau)$ can be modeled as

$$\mathbf{H}(\tau) = \sum_{l=1}^{L} \sqrt{\bar{p}_l} \left(\mathbf{R}_{\mathrm{Rx}}^{l}\right)^{\frac{1}{2}} \mathbf{G}_l \left(\mathbf{R}_{\mathrm{Tx}}^{l}\right)^{\frac{T}{2}} \delta\left[\tau - (l-1)\Delta\tau\right] \tag{27}$$

where $\mathbf{G}_l$ are random matrices with i.i.d. $\mathcal{CN}(0,1)$ elements and the average power $\bar{p}_l$ of each element can be modeled as shown in (25). Note that, in this paper, no path loss is considered; the normalization factor A in (25) is chosen such that (16) holds.

Using the model in (27), 1000 MIMO channel impulse response matrices are generated by Monte Carlo simulations for 2×2 and 3×3 setups and the discrete Fourier transform is used to obtain the frequency channel response. The cdf of the rms delay spread for the simulated SISO channel is plotted in the same figure as the measured data (see Fig. 7). The frequency correlation function $R(k,0)$ was estimated as $R(k,0) = (1/K)\sum_{i=1}^{K-k} h^H(f_i,t)h(f_{i+k},t)$, $k \geq 0$ [56], where $h(f_i,t)$ is the complex frequency response associated with frequency f_i at time t and K is the number of frequency subchannels. Averaging over both the time and spatial domains, Fig. 9 shows the averaged frequency correlation function from the measured data as well as that from the simulations. Both figures show that the simulation results match the measured data well. Finally, the capacity of the narrow-band MIMO channel is calculated and compared with that from the measured data (see Fig. 10). Good agreement between the measured data and the wide-band channel model is found.

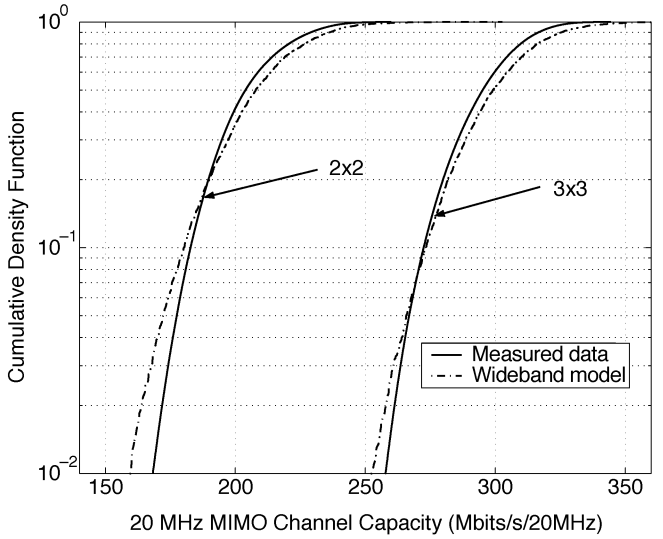

Fig. 11. The cdf of 20-MHz MIMO channel capacity. Power is equally allocated and the SNR at the receive side is 20 dB.

F. Simulations of 120-MHz MIMO Wireless Channels

The North American IEEE 802.11a and European HiperLAN/2 are two standards for high-speed wireless local area networks (WLAN). Both operate in the 5-GHz band and can provide high data rates between broadband core networks and mobile terminals. Both the IEEE 802.11a and HiperLAN/2 channels have 20-MHz bandwidth and use orthogonal frequency-division multiplexing (OFDM) technique. More details on the IEEE 802.11a and HiperLAN/2 standards can be found in [57] and [58].

For a system with 120-MHz bandwidth, six parallel 20 MHz channels can be provided. We use the above wide-band channel model to simulate a 120-MHz MIMO channel with 2×2 and 3×3 setups, where the covariance matrices for each tap at both ends are estimated from the measured data. The corresponding channel capacity is then calculated according to (15).

Fig. 11 shows the cdf of the capacity that one 20-MHz MIMO channel can provide with fully used 20-MHz bandwidth. There is a good agreement between the wide-band channel model

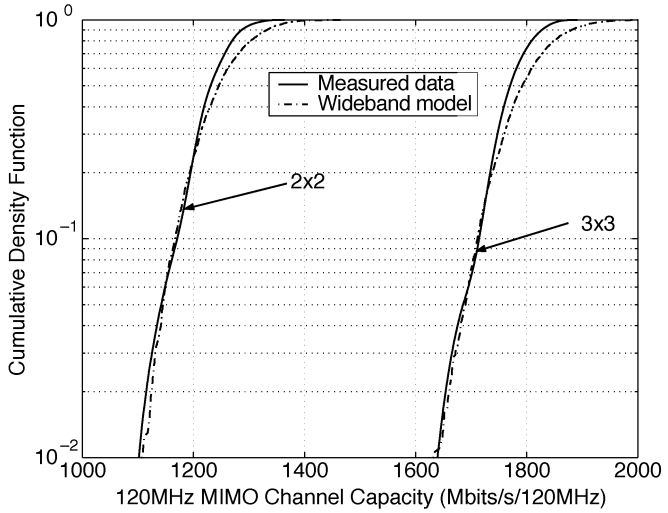

Fig. 12. The cdf of 120-MHz MIMO channel capacity. Power is equally allocated and the SNR at the receive side is 20 dB.

and the measured data. Furthermore, it is shown that, with 1% outage probability, one 20-MHz channel can provide capacity of approximately 170 Mbits/s (2 × 2 setup) and 250 Mbits/s (3 × 3 setup). These values match those reported in [59] well. It is also observed that the six parallel MIMO channels that are generated have similar capacity characteristics.

In Fig. 12, the capacity of the whole channel is plotted. Again, it is observed that the curves from the model fit the curves from the measured data well. The 1% outage channel capacity of the whole 120-MHz MIMO channel is above 1100 Mbits/s and 1600 Mbits/s for 2 × 2 and 3 × 3 setups, respectively. These numbers are higher than six times the capacity values of the 20-MHz MIMO channels shown in Fig. 11, which indicates the existence of frequency diversity gain (also see [7]).

VI. Conclusion and Discussion

This paper has reported results on statistical modeling of MIMO radio channels based on indoor measurements at 5.2 GHz. Both narrow- and wide-band channel models have been discussed. First, a previously proposed Kronecker structure-based narrow-band MIMO channel model has been verified from the measured data. It has been observed that the channel coefficients can be modeled by complex Gaussian variables for the measured NLoS indoor scenarios. Moreover, the MIMO channel covariance matrix can be well approximated by the Kronecker product of the covariance matrices seen from both ends. Concerning modeling the wide-band channels, it has been observed that the average power-delay profile of each element of the channel impulse response matrix agrees an exponential decay curve. Our investigation has also found that the Kronecker structure of the channel covariance matrix can be further extended to each wide-band channel tap. Therefore, we have proposed a wide-band MIMO channel model that combines a simple SISO channel model with the Kronecker structure. Monte Carlo simulations have been used and good agreement has been found by comparing the results from the measured data and those simulated using the above models.

The verification of the Kronecker structure of channel covariance matrix and the corresponding MIMO channel models provides support for many previously published results [34]–[36]. By decoupling the MIMO channel covariance matrix, some previously reported SIMO or MISO channel models [27] can now be used to model the covariance matrices at both transmitter and receiver. Furthermore, one can avoid expensive full MIMO channel measurements by measuring the corresponding SIMO/MISO channels at both ends.

Still, some open questions remain about these two models. For example, how to relate these two nonphysical models with some other well-known physical models? Under what conditions of the surrounding environment does the Kronecker structure of the second-order moments hold? In fact, the narrow-band MIMO channel model (13) is a special case of the distributed scattering model in [29]. Using the so-called ladder diagram in electromagnetic theory, a possible explanation on the Kronecker structure is given briefly [42] when the propagation media is diffusive. Also see [48] for a heuristic derivation of the Kronecker structure and more open problems.

Appendix

Finding the Permuted Version of (1): Rearranging the positions of the matrix elements to obtain a permuted version of (1) can be done by introducing a permutation matrix $\mathbf{P}$ such that

$$\mathbf{P}\,\mathrm{vec}(\mathbf{X}\otimes\mathbf{Y}) = \mathrm{vec}(\mathbf{x}\mathbf{y}^T) \tag{28}$$

where $\mathbf{X}$ and $\mathbf{Y}$ are two square matrices, $\mathbf{x} = \mathrm{vec}(\mathbf{X})$ and $\mathbf{y} = \mathrm{vec}(\mathbf{Y})$. It is obvious that there is a one-to-one mapping between the elements of $\mathrm{vec}(\mathbf{X}\otimes\mathbf{Y})$ and $\mathrm{vec}(\mathbf{x}\mathbf{y}^T)$ and that $\mathbf{P}$ is the corresponding permutation matrix. Then, the permuted matrix $\mathbf{R}_{\mathrm{perm}}$ can be obtained using the fact $\mathrm{vec}(\mathbf{R}_{\mathrm{perm}}) = \mathbf{P}\,\mathrm{vec}(\mathbf{R})$.

Without loss of generality, assume that $\mathbf{X}$ is an $m\times m$ matrix and that $\mathbf{Y}$ is an $n\times n$ matrix. Consequently, the dimensions for both $\mathrm{vec}(\mathbf{X}\otimes\mathbf{Y})$ and $\mathrm{vec}(\mathbf{x}\mathbf{y}^T)$ are $m^2n^2\times 1$.

Let us consider the position of $X_{ij}Y_{pq}$ in $\mathrm{vec}(\mathbf{X}\otimes\mathbf{Y})$ and $\mathrm{vec}(\mathbf{x}\mathbf{y}^T)$, respectively. Recall that

$$\mathbf{X}\otimes\mathbf{Y} = \begin{bmatrix} \mathbf{X}_{11}\mathbf{Y} & \cdots & \mathbf{X}_{1n}\mathbf{Y} \\ \vdots & \ddots & \vdots \\ \mathbf{X}_{m1}\mathbf{Y} & \cdots & \mathbf{X}_{mn}\mathbf{Y} \end{bmatrix}.$$

It is clear that $X_{ij}Y_{pq}$ is in row $n(i-1)+p$ and column $n(j-1)+q$ of $\mathbf{X}\otimes\mathbf{Y}$. Therefore, the index of $X_{ij}Y_{pq}$ in $\mathrm{vec}(\mathbf{X}\otimes\mathbf{Y})$ is

$$\begin{aligned} &nm\,[n(j-1)+q-1]+n(i-1)+p \\ &\qquad = n^2mj+nmq+ni+p-n^2m-nm-n. \end{aligned}$$

On the other hand, X_{ij} is in element $m(j-1)+i$ of $\mathbf{x}$ and Y_{pq} is in element $n(q-1)+p$ of $\mathbf{y}$. Obviously, $X_{ij}Y_{pq}$ is in row $m(j-1)+i$ and column $n(q-1)+p$ of $\mathbf{x}\mathbf{y}^T$. Therefore, the index of $X_{ij}Y_{pq}$ in $\mathrm{vec}(\mathbf{x}\mathbf{y}^T)$ is

$$\begin{aligned} &m^2\,[n(q-1)+p-1]+m(j-1)+i \\ &\qquad = m^2nq+m^2p+mj+i-m^2n-m^2-m. \end{aligned}$$

From the above results, the permutation matrix $\mathbf{P}$ is given as $P_{ab}=1$ for $a = m^2nq+m^2p+mj+i-m^2n-m^2-m$ and $b = n^2mj+nmq+ni+p-n^2m-nm-n$ while the rest of the elements of $\mathbf{P}$ are 0. Note that each row or column of $\mathbf{P}$ has only one element that equals 1 while the rest are 0. Therefore, $\mathbf{P}$ is orthonormal.

REFERENCES

[1] I. E.I. Emre Telatar, "Capacity of multi-antenna Gaussian channels," *Eur. Trans. Telecommun.*, vol. 10, no. 6, pp. 585–595, 1999.

[2] G. J. Foschini and M. J. Gans, "On limits of wireless communications in a fading environment," *Wireless Pers. Commun.*, vol. 6, pp. 311–335, 1998.

[3] L. H. Brandenburg and A. D. Wyner, "Capacity of the Gaussian channel with memory: The multivariate case," *Bell Syst. Tech. J.*, vol. 53, no. 5, pp. 745–778, 1974.

[4] D. P. McNamara, M. A. Beach, P. N. Fletcher, and P. Karlsson, "Initial investigation of multiple-input multiple-output channels in indoor environments," in *Proc. IEEE Benelux Chapter Symp. Communications and Vehicular Technology*, Leuven, Belgium, Oct. 2000, pp. 139–143.

[5] J. P. Kermoal, P. E. Mogensen, S. H. Jensen, and J. B. Andersen, "Experimental investigation of multipath richness for multi-element transmit and receive antenna arrays," in *Proc. IEEE VTC'00*, vol. 3, 2000, pp. 2004–2008.

[6] R. Stridh, P. Karlsson, and B. Ottersten, "MIMO channel capacity on a measured indoor radio channel at 5.8 GHz," in *Proc. Asilomar Conf. Signals, Systems and Computers*, vol. 1, Oct. 2000, pp. 733–737.

[7] A. F. Molisch, M. Steinbauer, M. Toeltsch, E. Bonek, and R. S. Thomä, "Capacity of MIMO systems based on measured wireless channels," *IEEE J. Select. Areas Commun.*, vol. 20, pp. 539–549, Apr. 2002.

[8] C. C. Martin, J. H. Winters, and N. R. Sollenberger, "Multiple-input multiple-output (MIMO) radio channel measurements," in *Proc. IEEE VTC'00*, vol. 2, 2000, pp. 774–779.

[9] J. W. Wallace and M. A. Jensen, "Spatial characteristics of the MIMO wireless channel: Experimental data acquisition and analysis," in *Proc. IEEE Int. Conf. Acoustics, Speech and Signal Processing*, vol. 4, 2001, pp. 2497–2500.

[10] P. Kyritsi, D. C. Cox, R. A. Valenzuela, and P. W. Wolniansky, "Effect of antenna polarization on the capacity of a multiple element system in an indoor environment," *IEEE J. Select. Areas Commun.*, vol. 20, pp. 1227–1239, Aug. 2002.

[11] V. Erceg, P. Soma, D. S. Baum, and A. J. Paulraj, "Capacity obtained from multiple-input multiple-output channel measurements in fixed wireless environments at 2.5 GHz," in *Proc. IEEE Int. Conf. Communications*, vol. 1, 2002, pp. 396–400.

[12] R. W. Heath Jr. and A. J. Paulraj, "Characterization of MIMO channels for spatial multiplexing systems," in *Proc. IEEE Int. Conf. Communications*, vol. 2, June 2001, pp. 591–595.

[13] R. U. Nabar, H. Bölcskei, V. Erceg, D. Gesbert, and A. J. Paulraj, "Performance of multiantenna signaling techniques in the presence of polarization diversity," *IEEE Trans. Signal Processing*, vol. 50, pp. 2553–2562, Oct. 2002.

[14] S. M. Alamouti, "A simple transmit diversity technique for wireless communications," *IEEE J. Select. Areas Commun.*, vol. 16, pp. 1451–1458, Oct. 1998.

[15] V. Tarokh, H. Jafarkhani, and A. R. Calderbank, "Space–time block codes from orthogonal designs," *IEEE Trans. Inform. Theory*, vol. 45, pp. 1456–1467, July 1999.

[16] V. Tarokh, N. Seshadri, and A. R. Calderbank, "Space–time codes for high data rate wireless communication: Performance criterion and code construction," *IEEE Trans. Inform. Theory*, vol. 44, pp. 744–765, Mar. 1998.

[17] G. Jöngren, M. Skoglund, and B. Ottersten, "Combining beamforming and orthogonal space–time block coding," *IEEE Trans. Inform. Theory*, vol. 48, pp. 611–627, Mar. 2002.

[18] G. Jöngren and M. Skoglund, "Improving orthogonal space–time block codes by utilizing quantized feedback information," in *Proc. IEEE Int. Symp. Information Theory*, June 2001, p. 220.

[19] G. G. Raleigh and J. M. Cioffi, "Spatio-temporal coding for wireless communication," *IEEE Trans. Commun.*, vol. 46, pp. 357–366, Mar. 1998.

[20] T. M. Cover and J. A. Thomas, *Elements of Information Theory*. New York: Wiley, 1991.

[21] P. A. Bello, "Characterization of randomly time-variant linear channels," *IEEE Trans. Commun. Syst.*, vol. CS-11, pp. 360–393, Dec. 1963.

[22] R. H. Clarke, "A statistical theory of mobile-radio reception," *Bell Syst. Tech. J*, vol. 47, no. 6, pp. 957–1000, 1968.

[23] W. C. Jakes, Ed., *Microwave Mobile Communications*. New York: Wiley, 1974.

[24] A. Saleh and R. Valenzuela, "A statistical model for indoor multipath propagation," *IEEE J. Select. Areas Commun.*, vol. SAC-5, pp. 128–137, Feb. 1987.

[25] T. S. Rapport, S. Y. Seidel, and K. Takamizawa, "Statistical channel impulse response models for factory and open plan building radio communication system design," *IEEE Trans. Commun.*, vol. 39, pp. 794–807, May 1991.

[26] H. Hashemi, "Impulse response modeling of indoor radio propagation channels," *IEEE J. Select. Areas Commun.*, vol. 11, pp. 967–978, Sept. 1993.

[27] R. B. Ertel, P. Cardieri, K. W. Sowerby, T. S. Rappaport, and J. H. Reed, "Overview of spatial channel models for antenna array communication systems," *IEEE Pers. Commun.*, vol. 5, pp. 10–22, Feb. 1998.

[28] D.-S. Shiu, G. J. Foschini, M. J. Gans, and J. M. Kahn, "Fading correlation and its effect on the capacity of multielement antenna systems," *IEEE Trans. Commun.*, vol. 48, pp. 502–513, Mar. 2000.

[29] D. Gesbert, H. Bölcskei, D. A. Gore, and A. Paulraj, "Outdoor MIMO wireless channels: Models and performance prediction," *IEEE Trans. Commun.*, vol. 50, pp. 1926–1934, Dec. 2002.

[30] D. Chizhik, G. J. Foschini, and R. A. Valenzuela, "Capacities of multi-element transmit and receive antennas: Correlation and keyholes," *Electron. Lett.*, vol. 36, no. 13, pp. 1099–1100, 2000.

[31] K. I. Pedersen, J. B. Andersen, J. P. Kermoal, and P. Mogensen, "A stochastic multiple-input–multiple-output radio channel model for evaluation of space–time coding algorithms," in *Proc. IEEE VTC'00*, vol. 2, 2000, pp. 893–897.

[32] J. P. Kermoal, L. Schumacher, K. I. Pedersen, P. E. Mogensen, and F. Frederiksen, "A stochastic MIMO radio channel model with experimental validation," *IEEE J. Select. Areas Commun.*, vol. 20, pp. 1211–1226, Aug. 2002.

[33] K. Yu and B. Ottersten, "Models for MIMO propagation channels, a review," *J. Wireless Commun. Mobile Comput.*, vol. 2, no. 7, pp. 553–666, 2002.

[34] D. Chizhik, F. Rashid-Farrokhi, J. Ling, and A. Lozano, "Effect of antenna separation on the capacity of BLAST of correlated channels," *IEEE Commun. Lett.*, vol. 4, pp. 337–339, Nov. 2000.

[35] C. Martin and B. Ottersten, "Analytic approximations of eigenvalue moments and mean channel capacity for MIMO channels," in *Proc. IEEE Int. Conf. Acoustics, Speech and Signal Processing (ICASSP)*, vol. 3, May 2002, pp. 2389–2392.

[36] H. Bölcskei, M. Borgmann, and A. J. Paulraj, "Performance of space-frequency coded broadband OFDM under real-world propagation conditions," in *Proc. Eur. Conf. Signal Processing (EUSIPCO)*, Sept. 2002.

[37] P. Karlsson, D. McNamara, and M. Beach, Indoor and campus single and dual multi-sensor channel characterization: measurement data, part 2: Indoor dual multi-sensor characterization data, in European Union IST Program Smart Antenna Technology in Universal Broadband Wireless Networks Project, IST-1999-10322, Deliverable 522, Part 2, Oct. 2000.

[38] K. Yu, M. Bengtsson, B. Ottersten, D. McNamara, P. Karlsson, and M. Beach, "Second order statistics of NLOS indoor MIMO channels based on 5.2 GHz measurements," in *Proc. IEEE Global Telecommunications Conf.*, vol. 1, Nov. 2001, pp. 156–160.

[39] C. Van Loan and N. Pitsianis, "Approximation with Kronecker products," in *Linear Algebra for Large Scale and Real Time Applications*, M. S. Moonen, G. H. Golub, and B. L. R. De Moor, Eds. Norwell, MA: Kluwer, 1993, pp. 293–314.

[40] G. H. Golub and C. F. Van Loan, *Matrix Computations*, 3rd ed. Baltimore, MD: The Johns Hopkins Univ. Press, 1996.

[41] R. A. Horn and C. R. Johnson, *Matrix Analysis*. Cambridge, U.K.: Cambridge Univ. Press, 1985.

[42] A. L. Moustakas, H. U. Baranger, L. Balents, A. M. Sengupta, and S. H. Simon, "Communication through a diffusive medium: Coherence and capacity," *Sci.*, vol. 287, pp. 287–290, 2000.

[43] C.-N. Chuah, D. N. C. Tse, J. M. Kahn, and R. A. Valenzuela, "Capacity scaling in MIMO wireless systems under correlated fading," *IEEE Trans. Inform. Theory*, vol. 48, pp. 637–650, Mar. 2002.

[44] G. L. Stuber, *Principles of Mobile Communication*. Norwell, MA: Kluwer, 1996.

[45] T. S. Rappaport, *Wireless Communications, Principles and Practice*. Englewood Cliffs, NJ: Prentice-Hall, 1996.

[46] S. M. Kay, *Fundamentals of Statistical Signal Processing: Estimation Theory*. Englewood Cliffs, NJ: Prentice-Hall, 1993, vol. 1.

[47] A. Graham, *Kronecker Products and Matrix Calculus With Applications*. Chichester, U.K.: Ellis Horwood, 1981.

[48] M. Bengtsson, K. Yu, and B. Ottersten, Single and dual multi-sensor channel characterization—Analysis and models: Stochastic models, in European Union IST Program Smart Antenna Technology in Universal Broadband Wireless Networks Project, IST-1999-10322, Deliverable 523, Part I, ver. 2.0, Nov. 2001.

[49] D. P. Palomar, J. R. Fonollosa, and M. A. Lagunas, "Capacity results of spatially correlated frequency-selective MIMO channels in UMTS," in *Proc. IEEE VTC'01*, vol. 2, 2001, pp. 553–557.

[50] L. Schumacher, L. T. Berger, and J. Ramiro-Moreno, "Recent advances in propagation characterization and multiple antenna processing in the 3GPP framework," in *Proc. XXVIIth Triennial General Assembly of the Int. Union of Radio Science (URSI)*, Aug. 2002.

[51] J. Medbo, H. Andersson, P. Schramm, H. Asplund, and J. E. Berg, Channel models for HIPERLAN/2 in different indoor scenarios, in COST 259 TD(98)70, Apr. 1998.

[52] R. Ganesh and K. Pahlavan, "Statistical modeling and computer simulation of indoor radio channel," *Inst. Elect. Eng. Proc.—I*, vol. 138, no. 3, pp. 153–161, 1991.

[53] K. I. Pedersen, P. E. Mogensen, and B. H. Fleury, "A stochastic model of the temporal and azimuthal dispersion seen at the base station in outdoor propagation environments," *IEEE Trans. Veh. Technol.*, vol. 49, pp. 437–447, Mar. 2000.
[54] D. Molkdar, "Review on radio propagation into and within buildings," *Inst. Elect. Eng. Proc.—H*, vol. 138, no. 1, pp. 61–73, 1991.
[55] C. Bergljung and P. Karlsson, "Propagation characteristics for indoor broadband radio access networks in the 5 GHz band," in *Proc. IEEE 9th Int. Symp. Personal, Indoor and Mobile Radio Communications*, vol. 2, 1998, pp. 612–616.
[56] K. Pahlavan and A. H. Levesque, *Wireless Information Networks*. New York: Wiley, 1995.
[57] *Wireless LAN medium access control (MAC) and physical layer (PHY) specifications: High-speed physical layer in the 5-GHz band*, IEEE Std. 802.11a, Sept. 1999.
[58] ETSI, Broadband radio access networks (BRAN); HIPERLAN Type 2; physical layer, Tech. rep. ETSI TS 101 475 V1.2.2 (2001–2002), 2001.
[59] K. Yu, M. Bengtsson, B. Ottersten, D. McNamara, P. Karlsson, and M. Beach, "A 20 MHz HiperLAN/2 MIMO channel model in NLOS indoor scenarios," in *Proc. Konferensen RadioVetenskap och Kommunikation (RVK) '02*, 2002, pp. 311–315.

Kai Yu (S'01) received the B.Eng. degree from Shanghai University, Shanghai, China, in 1998 and the M.Sc. degree (with distinction) from the University of Liverpool, Liverpool, U.K., in 2000, both in electrical engineering, and the Tech. Lic. degree from the Royal Institute of Technology (KTH), Stockholm, Sweden, in 2002, where he is currently working toward the Ph.D. degree in signal processing.

From March to September 2003, he was a Visiting Researcher at the Smart Antennas Research Group, Stanford University, Stanford, CA. His current research interests include multiple-input–multiple-output (MIMO) channel modeling, array signal processing, and multiple access techniques.

Mats Bengtsson (S'96–M'00) received the M.S. degree in computer science from Linköping University, Linköping, Sweden, in 1991 and the Tech. Lic. and Ph.D. degrees in electrical engineering from the Royal Institute of Technology (KTH), Stockholm, Sweden, in 1997 and 2000, respectively.

He was with Ericsson Telecom AB Karlstad, Sweden, from 1991 to 1995 and is currently with the KTH as a Research Associate. His research interests include statistical signal processing and its applications to antenna array processing and communications, radio resource management, and propagation channel modeling.

Björn Ottersten (S'87–M'89–SM'99–F'04) was born in Stockholm, Sweden, in 1961. He received the M.S. degree in electrical engineering and applied physics from Linköping University, Linköping, Sweden, in 1986 and the Ph.D. degree in electrical engineering from Stanford University, Stanford, CA, in 1989.

He has held research positions at the Department of Electrical Engineering, Linköping University, and the Information Systems Laboratory, Stanford University. In 1991, he was appointed Professor of Signal Processing at KTH. From 1996 to 1997, he was Director of Research at ArrayComm Inc, San Jose, CA. He currently is the Head of the Department of Signals, Sensors and Systems, Royal Institute of Technology (KTH), Stockholm, Sweden. He also is a Visiting Professor at the Katholieke Universiteit Leuven, Leuven, Belgium, and the University of Luxembourg, Luxembourg. His research interests include wireless communications, stochastic signal processing, sensor array processing, and time series analysis.

Dr. Ottersten has authored papers that received the Signal Processing Society Paper Award in 1993 and 2001. He is Coeditor-in-chief of *EURASIP Signal Processing Journal*, Associate Editor for the IEEE TRANSACTIONS ON SIGNAL PROCESSING, and a Member of the editorial boards of IEEE SIGNAL PROCESSING MAGAZINE and *EURASIP Journal of Applied Signal Processing*.

Darren McNamara received the M.Eng. degree in electrical and electronic engineering from the University of Bristol, Bristol, U.K., in 1999. He received the Ph.D. degree, also from the University of Bristol, in the area of multiple-input–multiple-output (MIMO) channel measurement and analysis in 2003.

During his studies, he was sponsored by Racal Radio, Ltd., Seaton, U.K., where he followed their graduate training program and worked on wireless remote ground sensor systems. During the course of this work, he was involved with the IST Smart Antenna Technology in Universal Broadband Wireless Networks project and the activities of COST273. Since November 2002, he has been with the Toshiba Telecommunications Research Laboratory, Bristol, U.K.

Peter Karlsson received the M.Sc. and Ph.D. degrees from the Lund Institute of Technology, Lund, Sweden, in 1988 and 1995, respectively.

He joined the Radio System Group, Telia Research AB, Malmö, Sweden, in 1995, working on design, analysis, and trials with high-capacity mobile and fixed broadband radio communications systems. He has been contributing to the standardization of UMTS in Third Generation Partnership Project (3GPP) and the 5-GHz wireless local area networks (WLANs) in ETSI BRAN and IEEE 802.11 physical layer, focusing on channels models and range extension with smart antennas. He was a Research Fellow at the University of Bristol, Bristol, U.K., in 2000 in combination with a part-time position at Telia Research, Malmö, Sweden, working with adaptive antennas both for cellular and WLAN systems, where he was appointed Expert in Radio Communications in 2001. He currently holds the Expert position at TeliaSonera Sweden, Mobile Network R&D. He has written and coauthored approximately 50 conference and journal papers on antennas and propagation and on mobile and fixed radio systems.

Dr. Karlsson chaired the HiperLAN2 Global Forum (H2GF) Regulatory Group from 1999 to 2001, which aimed at global allocation for WLANs in the 5-GHz band. He is active in long-term University research cooperation and is Chairman of the Swedish PCC++ Board and in the steering group of the Wireless@KTH Affordable Wireless Service Infrastructure Program.

Mark Beach received the Ph.D. degree for research addressing the application of smart antennas to global positioning systems (GPS) from the University of Bristol, Bristol, U.K.

He joined the University of Bristol as a Member of Academic Staff in 1989, where he currently is Professor of Radio Systems Engineering. His research interest in smart-antenna techniques has continued with the application of dual array techniques (MIMO architectures) to high-performance wireless networks. Further, he has conducted novel research in the area of analog radio frequency (RF) technologies for software definable, or reconfigurable, radio, such as linearized mixers and tunable RF filters under E.U. projects such as TRUST and SCOUT.

Dr. Beach is an active Member of the Institution of Electrical Engineers Professional Network on Antennas and Propagation, as well as an Editor for the IEEE TRANSACTIONS ON WIRELESS COMMUNICATIONS.